Cell Reports
Physical Science

CellPress
OPEN ACCESS

Report

Efficient and stable $CsPbI_3$ perovskite solar cells with spontaneously formed 2D-$Cs_2PbI_2Cl_2$ at the buried interface

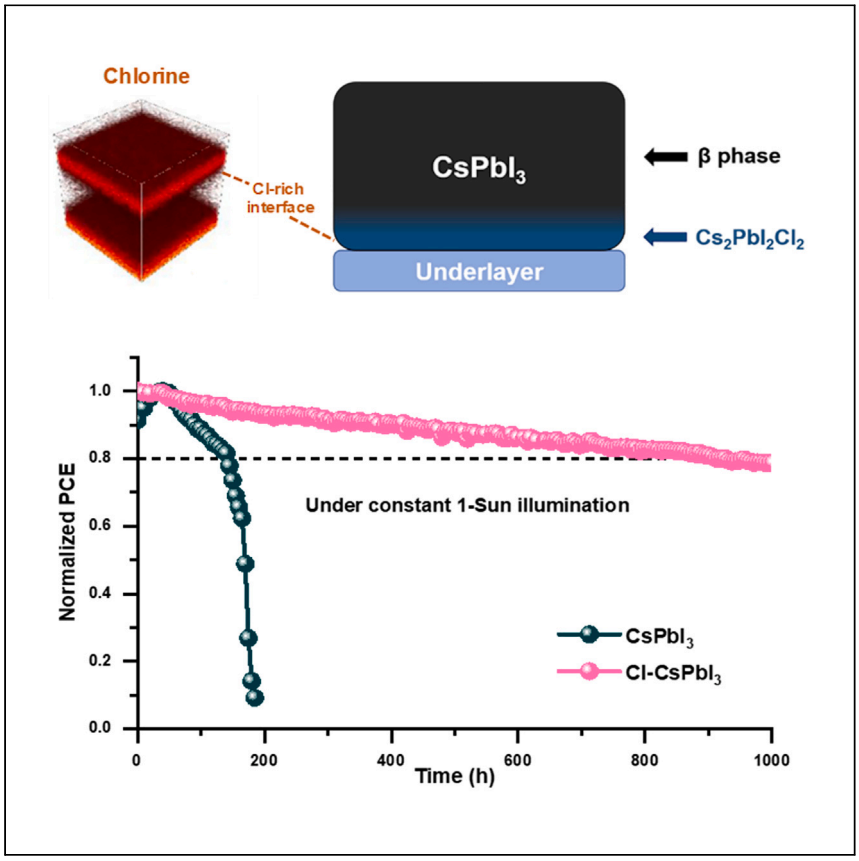

By employing a Cl-containing $CsPbI_3$ precursor, Shah et al. report the spontaneously formed 2D Ruddlesden-Popper $Cs_2PbI_2Cl_2$ at the buried interface. The resulting devices exhibit a power conversion efficiency of 20.6% and show remarkable stability under constant 1-sun illumination, retaining 80% of their initial efficiency after 1,000 h.

Syed-Fawad-Ali Shah, Inyoung Jeong, Jaewang Park, ..., Sang Il Seok, Kihwan Kim, Hanul Min

joopark@kier.re.kr (J.H.P.)
seoksi@unist.ac.kr (S.I.S.)
kimkh@kier.re.kr (K.K.)
hmin92@korea.ac.kr (H.M.)

Highlights

Stable inorganic perovskites have been successfully fabricated

Interface engineering plays an essential role in the stability of $CsPbI_3$ solar cells

The significance of precise control over dopant redistribution has been demonstrated

Shah et al., Cell Reports Physical Science 5, 101935
May 15, 2024
https://doi.org/10.1016/j.xcrp.2024.101935

Cell Reports
Physical Science

CellPress
OPEN ACCESS

Report

Efficient and stable $CsPbI_3$ perovskite solar cells with spontaneously formed 2D-$Cs_2PbI_2Cl_2$ at the buried interface

Syed-Fawad-Ali Shah,[1,2] Inyoung Jeong,[1] Jaewang Park,[3] Donghyeop Shin,[1,2] Inchan Hwang,[1] Nikolai Tsvetkov,[4] Dohyung Kim,[5] Jihye Gwak,[1,2] Joo Hyung Park,[1,2,*] Sang Il Seok,[3,*] Kihwan Kim,[1,2,*] and Hanul Min[4,6,7,*]

SUMMARY

Despite its nature of superior thermal and photostability compared to the mixed cation or halide counterparts, cesium lead triiodide ($CsPbI_3$) suffers from the undesired phase transition from β phase to δ phase, which is often initiated at the buried interface. In this study, we demonstrate that the addition of Cl induces the spontaneous formation of the two-dimensional (2D) Ruddlesden-Popper (RP) phase of $Cs_2PbI_2Cl_2$. The 2D RP $Cs_2PbI_2Cl_2$ predominantly forms at the buried interface due to Cl segregation, improving the electron transfer and phase stability of the $CsPbI_3$ thin films. Perovskite solar cells based on $CsPbI_3/Cs_2PbI_2Cl_2$ light absorbers exhibited a power conversion efficiency (PCE) of 20.6% (with a stabilized efficiency of 20.1%) under simulated solar illumination. Furthermore, the unencapsulated devices retained approximately 80% of their initial PCEs after continuous light exposure for 1,000 h.

INTRODUCTION

Cesium lead triiodide ($CsPbI_3$) presents a band gap of 1.68–1.70 eV and avoids mixed cation or halide segregation, thereby making it a promising top-cell candidate in tandem solar cells or indoor photovoltaic applications.[1–3] The power conversion efficiency (PCE) of $CsPbI_3$-based single-junction solar cells has been increased to more than 20% by improving the surface morphology,[4] passivating the $CsPbI_3$ interfaces,[5] forming phase heterojunctions,[6] and regulating the phase conversion process.[7] More recently, effective strategies, such as suppressing ion migration,[8] stabilizing the precursor solution,[9] and using bifacial defect passivators, have been employed,[10] achieving a PCE even surpassing 21%, making them comparable to mixed halide wide band-gap perovskites. However, $CsPbI_3$ often suffers from inferior phase stability under ambient conditions despite having superior chemical and thermal stabilities compared to its hybrid counterparts.

Various strategies employed for improving the phase stability of $CsPbI_3$ or formamidinium lead triiodide include the use of mixed cations (e.g., methylammonium) and halides (e.g., Br or Cl)[11,12] or the formation of junctions with two-dimensional (2D) perovskites at the interface or bulk.[13–15] Efforts to enhance the phase stability and reduce interfacial defects have focused primarily on top-surface passivation of perovskite using longer cation chains with high hydrophobicity.[14,16] However, the need for modification of the buried interface has recently arisen for improving the stability and efficiency of $CsPbI_3$-based solar cells because the undesired phase transformation from the black α, β, or γ phase to the yellow δ phase is often initiated

[1]Photovoltaic Research Department, Korea Institute of Energy Research, Daejeon 34129, South Korea

[2]Renewable Energy Engineering, University of Science and Technology, Daejeon 34113, South Korea

[3]Department of Energy and Chemical Engineering, Ulsan National Institute of Science and Technology, Ulsan 44919, South Korea

[4]KU-KIST Graduate School of Converging Science and Technology, Korea University, Seoul 02841, South Korea

[5]Department of Advanced Materials Engineering, Chungbuk National University, Cheongju 28644, South Korea

[6]Department of Integrative Energy Engineering, Korea University, Seoul 02841, South Korea

[7]Lead contact

*Correspondence: joopark@kier.re.kr (J.H.P.), seoksi@unist.ac.kr (S.I.S.), kimkh@kier.re.kr (K.K.), hmin92@korea.ac.kr (H.M.)

https://doi.org/10.1016/j.xcrp.2024.101935

near the buried interface and is propagated toward the surface.[17,18] Liu et al. reported that the introduction of alkyltrimethoxysilane at the perovskite/TiO_2 interface enhanced the electron transfer and improved the phase stability by reducing the interfacial lattice distortion.[17] Xu et al. optimized the conductivity, electron mobility, and energy band structure of the perovskite/TiO_2 interface by tailoring it with amino-2,3,5,6-tetrafluorobenzoate cesium.[19] Furthermore, the modification of the buried interface can lead to the passivation of interfacial defects and facilitate perovskite crystallization.[18,20] Thus, the formation of a 2D Ruddlesden-Popper (RP)-phase perovskite at the buried interface can reduce interfacial defects, optimize band alignment, and improve phase stability. However, passivating the buried interface with a 2D perovskite is difficult because the 2D perovskite layer may dissolve when coating the three-dimensional (3D) perovskite layer. Alternatively, the dissolution issue may not be a concern if the 2D perovskite can be formed spontaneously at the buried interface during the formation of the 3D perovskite layer.

The 2D RP phase of $Cs_2PbI_2Cl_2$ exhibits excellent thermodynamic stability,[21] has a high carrier mobility,[22] and is a good lattice match with $CsPbX_3$,[23] making it a promising passivation agent for $CsPbI_3$. Zhao et al. reported that an all-inorganic 2D $Cs_2PbI_2Cl_2$ capping layer on the $CsPbI_3$ surface remarkably improved the long-term stability of the devices.[16] In addition, the interface passivation with synthesized $Cs_2PbI_2Cl_2$ nanosheets enhanced both stability and efficiency of the $CsPbI_2Br$-based solar cells.[24] However, the 3D perovskite coating solution may dissolve the preformed $Cs_2PbI_2Cl_2$ layer and suffer from low wettability.

To enhance the efficiency and stability of $CsPbI_3$-based perovskite solar cells (PSCs), it is highly desirable to employ buried interface passivation involving a 2D RP phase with favorable compatibility, such as $Cs_2PbI_2Cl_2$. In this study, we demonstrate the spontaneous formation of a $Cs_2PbI_2Cl_2$ layer at the buried interface without additional processes. As reported previously, Cl anions are segregated at the buried interface when a Cl-containing perovskite precursor is employed.[25] Moreover, Cl-containing $CsPbI_3$ preferentially forms a $Cs_2PbI_2Cl_2/CsPbI_3$ heterojunction rather than a homogeneous 3D $CsPbI_{3-x}Cl_x$ phase.[23,26] The presence of $Cs_2PbI_2Cl_2$ at the buried interface enhanced charge extraction and improved the crystallinity of the absorber layer, leading to an increase in the PCE of the $CsPbI_3$-based solar cells from 18.9% to 20.6%. Importantly, the Cl-containing $CsPbI_3$ showed phase stability superior to the pristine-$CsPbI_3$, Br-containing $CsPbI_3$, and Br/Cl-containing $CsPbI_3$, retaining 80% of its initial efficiency after 1,000 h of continuous light exposure.

RESULTS AND DISCUSSION

Fabrication and characterization of $CsPbI_3$-based films

To form β-$CsPbI_3$ perovskite thin films, we employed the solution-based method[1] by carefully controlling the halide ratios. Figure 1A shows the 3D redistribution of Cl^- obtained by time-of-flight secondary-ion mass spectrometry (ToF-SIMS) for pristine-$CsPbI_3$, $CsPbI_3$ with 20 mol % Br (denoted as Br-$CsPbI_3$), $CsPbI_3$ with 15 mol % Cl (denoted as Cl-$CsPbI_3$), and $CsPbI_3$ with 20 mol % Br and 15 mol % Cl (denoted as Br/Cl-$CsPbI_3$) on a compact TiO_2 (c-TiO_2)/fluorine-doped tin oxide (FTO)/glass substrate (the full anion-targeted ToF-SIMS depth profiles are displayed in Figure S1). As reported previously, the Cl^- anions are segregated at the buried interface between $CsPbI_3$ and c-TiO_2 in Cl-$CsPbI_3$ and Br/Cl-$CsPbI_3$, while the iodide ions are distributed uniformly. Therefore, the ratio of chloride to iodide anions at the buried interface was 1:1 or higher. Additionally, although it has been reported that dimethyl-ammonium iodide (DMAI) can sublimate at approximately 170°C,[1,27] our

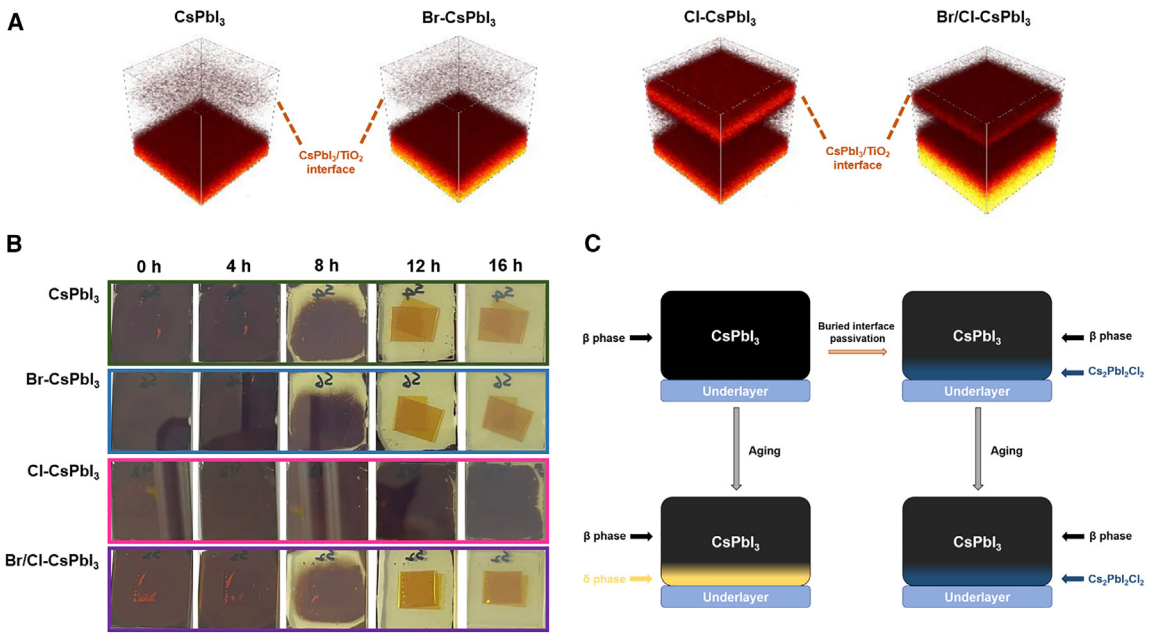

Figure 1. Impact of Cl addition on $CsPbI_3$ films

(A) ToF-SIMS targeting Cl^- within FTO/c-TiO_2/perovskite of $CsPbI_3$, Br-$CsPbI_3$, Cl-$CsPbI_3$, and Br/Cl-$CsPbI_3$.

(B) Photographic images of $CsPbI_3$, Br-$CsPbI_3$, Cl-$CsPbI_3$, and Br/Cl-$CsPbI_3$ perovskite films with respect to exposure time under 25°C and 65 RH%.

(C) Schematic demonstrating the suppression of phase degradation with and without $Cs_2PbI_2Cl_2$ at the buried interface.

ToF-SIMS and Fourier transform infrared results (Figure S2) indicate that $CsPbI_3$ films may contain trace amounts of organic components, which is consistent with previously reported $Cs_xDMA_{1-x}PbI_3$ ToF-SIMS results.[1]

Bare perovskite thin films are usually susceptible to moisture, exhibiting relatively poor stability (Figure S3). Therefore, recently, hydrophobic surface passivation is widely employed.[4] Figure 1B shows the photographs of the n-octylammonium iodide (OAI) passivated perovskite films exposed to 65% relative humidity (RH) at 25°C. Although the perovskite layer was passivated by the hydrophobic OAI, the pristine-$CsPbI_3$ showed poor phase stability, changing to the yellow δ phase after 8 h. It is widely known that the addition of bromide to pure iodide perovskites can improve their stability due to the increased ionic strength.[11,28,29] However, Br-$CsPbI_3$ showed a stability similar to that of with $CsPbI_3$, which can be attributed to the insufficient addition of Br. Addition of a large amount of Br is not advisable because it causes an undesirable change in the band gap. As shown in Figure S4, the band gaps of Br-$CsPbI_3$ and Br/Cl-$CsPbI_3$ were blueshifted compared to that of $CsPbI_3$, whereas the band gap change in Cl-$CsPbI_3$ was negligible. The Cl-$CsPbI_3$ sample maintained its black phase even after 16 h of exposure. Since Cl is difficult to be fully incorporated in the lattice of pure iodide perovskites[25,26,30] and is segregated at the buried interface, the improved stability can be attributed to the formation of a unique phase, such as $Cs_2PbI_2Cl_2$ at the buried interface, as depicted by the schematic in Figure 1C. Concurrently, the stability of Br/Cl-$CsPbI_3$ was relatively poor, showing a stability similar to that of $CsPbI_3$ and Br-$CsPbI_3$ and as compared to that of Cl-$CsPbI_3$. Although Cl was segregated at the buried interface in Br/Cl-$CsPbI_3$, the difference in the Cl content between the perovskite surface and the buried interface was relatively small compared to that in the case of Cl-$CsPbI_3$ (Figure S1). It has been previously reported that Cl can be incorporated into perovskite lattices in which iodide and Br exist together.[31] Furthermore, Akkerman et al.[26]

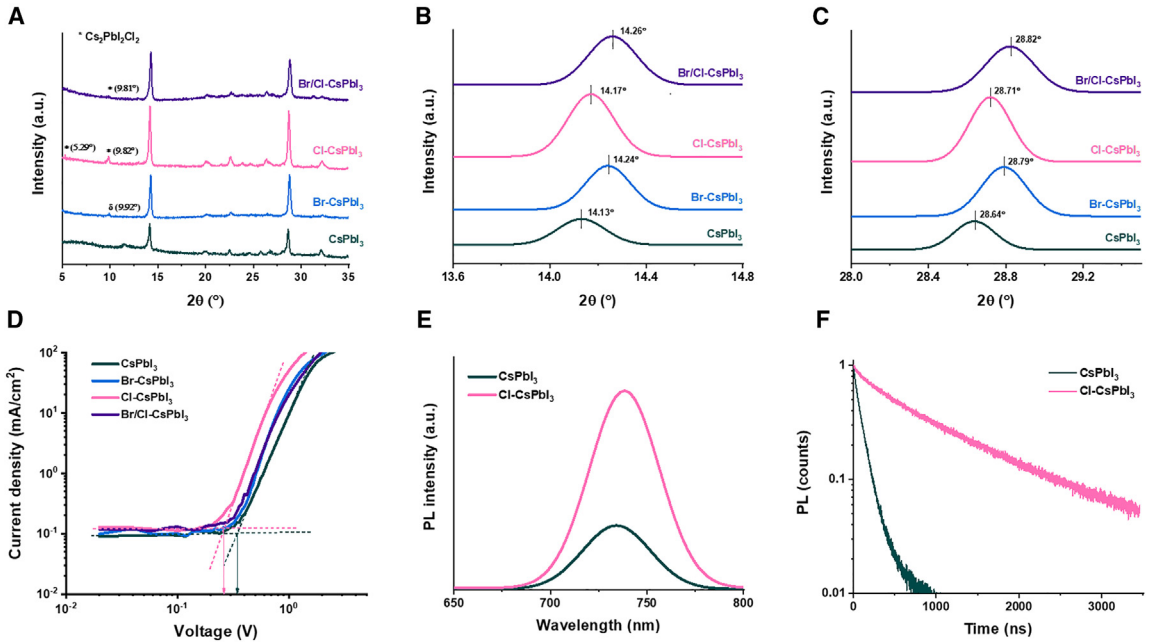

Figure 2. Structural and optoelectronic properties of perovskite

(A) XRD patterns of $CsPbI_3$, Br-$CsPbI_3$, Cl-$CsPbI_3$, and Br/Cl-$CsPbI_3$.

(B and C) Magnified (B) (100) and (C) (200) plane diffraction peaks in (A).

(D) Dark *J-V* curves of electron-only devices.

(E and F) Steady-state PL spectra (E) and TCSPC (F) of glass substrate/perovskite films of $CsPbI_3$ and Cl-$CsPbI_3$ with an excitation wavelength of 635 nm.

reported that, when Cl/Br/I halides were mixed at a 1:1:1 ratio, $CsPb(Cl:Br:I)_3$ was formed with a small amount of iodide-containing $CsPbBr_2Cl$. Thus, the addition of Br to the Cl/iodide-containing $CsPbI_3$ can suppress the formation of $Cs_2PbI_2Cl_2$.

To confirm the formation of $Cs_2PbI_2Cl_2$, we analyzed the X-ray diffraction (XRD) patterns of the peeled-off $CsPbI_3$, Br-$CsPbI_3$, Cl-$CsPbI_3$, and Br/Cl-$CsPbI_3$ perovskite layers (Figure 2A). All perovskite layers showed the β phase of $CsPbI_3$ with two dominant peaks near 14° and 28°, which can be assigned to the β(100) and β(200) crystal planes, respectively. In general, well-oriented and textured films with strong XRD peaks indicate the high crystallinity of the samples, which is beneficial for charge transport and electron extraction. Among the samples, the Cl-$CsPbI_3$ sample showed the highest XRD peak intensity. Furthermore, two additional peaks at 5.39° and 9.82° were observed in the XRD pattern of Cl-$CsPbI_3$ which can be assigned to the 2D RP $Cs_2PbI_2Cl_2$ phase.[16,21,32,33] A trace amount of $Cs_2PbI_2Cl_2$ was observed in the Br/Cl-$CsPbI_3$ sample, while a small amount of δ-phase $CsPbI_3$ was observed in Br-$CsPbI_3$. These results imply that the formation of a stable 2D RP $Cs_2PbI_2Cl_2$ phase at the buried interface contributed to the enhanced β-phase stability of Cl-$CsPbI_3$.

When a small amount of Br or Cl is incorporated into the lattice of an iodide-based perovskite, the cubic perovskite structure shrinks, and the XRD peak shifts to higher angles. The peak at 14.13° in the XRD pattern of $CsPbI_3$ shifted to 14.24° in that of Br-$CsPbI_3$, indicating that Br^- ions were successfully incorporated into the $CsPbI_3$ lattice, inducing lattice shrinkage (Figures 2B and 2C). Despite the smaller ionic radius of Cl than that of Br, the peak shift in Cl-$CsPbI_3$ was less pronounced than in Br-$CsPbI_3$, which gives additional confirmation that the Cl ion is not fully

incorporated into the iodide-based perovskite lattice. In Br/Cl-$CsPbI_3$, the most prominent XRD peak shift was observed, indicating the coexistence of triple halides.

Undesirable lattice distortion of perovskite and phase transition may induce defects that can capture and trap free charge carriers.[34,35] To quantitatively assess the defect density, we fabricated electron- and hole-only devices with a configuration of FTO/c-TiO_2/perovskite/C60/bathocuproine/Ag (Figure 2D) and FTO/poly(triaryl amine)/perovskite/2,2′,7,7′-tetrakis[N,N-di(4-methoxyphenyl)amino]-9,9′-spirobifluorene (Spiro-OMeTAD)/Au (Figure S5), respectively, and characterized the evolution of the space-charge-limited current (SCLC). The defect density was calculated by using the equation $N_{defects} = 2\varepsilon\varepsilon_0 V_{TFL}/eL$,[2] where ε and ε_0 represent the dielectric constant of $CsPbI_3$ and vacuum permittivity, respectively; L is the thickness of the perovskite films; and e is the elementary charge. The calculated electron trap densities of $CsPbI_3$, Br-$CsPbI_3$, Cl-$CsPbI_3$, and Br/Cl-$CsPbI_3$ were 6.4×10^{14}, 6.2×10^{14}, 4.7×10^{14}, and 5.6×10^{14} cm^{-3}, respectively, and the hole trap densities were 4.0×10^{14}, 2.3×10^{14}, 2.2×10^{14}, and 5.5×10^{14} cm^{-3}, respectively. In addition, the charge carrier mobility was calculated using the Mott-Gurney equation: $J = [9\varepsilon\mu(V\text{-}V_{Bi})^2]/[8L^3]$, where J is the current density; V and V_{Bi} are the applied and built-in voltages, respectively; ε is the dielectric constant; L is the thickness; and μ is the mobility. The value of electron mobility was the highest for Cl-$CsPbI_3$ (2.2 $cm^2\ V^{-1}\ s^{-1}$) compared to those for $CsPbI_3$ (1.5 $cm^2\ V^{-1}\ s^{-1}$), Br-$CsPbI_3$ (2.0 $cm^2\ V^{-1}\ s^{-1}$), and Br/Cl-$CsPbI_3$ (1.7 $cm^2\ V^{-1}\ s^{-1}$).

Optoelectronic properties of perovskite films

Figure 2E depicts the steady-state photoluminescence (PL) spectra of $CsPbI_3$ and Cl-$CsPbI_3$ on a glass substrate using 635-nm excitation. The perovskite films prepared with Cl-$CsPbI_3$ exhibited a lower trap density and higher PL intensity than that prepared with $CsPbI_3$. In addition, time-correlated single-photon counting (TCSPC) measurements were performed to compare the charge recombination rates in the samples (Figure 2F). The carrier lifetime values were obtained using the bi-exponential equation $Y = A_1 exp(-t/\tau_1) + A_2 exp(-t/\tau_2)$, where τ_1 and τ_2 denote the fast and slow decay time and are related to the trap-assisted non-radiative and radiative recombination processes, respectively. The carrier lifetime of Cl-$CsPbI_3$ was 1,050 ns, which was significantly longer than that of $CsPbI_3$ (230 ns). The SCLC, steady-state PL, and TCSPC were in good agreement and imply that Cl-$CsPbI_3$ possess fewer trap sites compared to $CsPbI_3$.

$Cs_2PbI_2Cl_2$ may enhance the charge carrier extraction owing to its proper energy level,[24] a higher charge carrier mobility,[22] and a good lattice match with $CsPbI_3$[23]. By using the equation $F(x) = F(x_0)e^{-\alpha(x\text{-}xo)}$, where $F(x)$ is the intensity at a point x below the surface of the layer, $F(x_0)$ is the intensity at the surface x_0, and α is the absorption coefficient, which was calculated from the UV-visible (UV-vis) absorption spectra, we were able to calculate the penetration depth at each excitation wavelength (Figures S6A and S6B). Although Cl-$CsPbI_3$ showed a higher steady-state PL intensity than $CsPbI_3$ on the glass substrate, it showed a considerably lower PL intensity on the FTO/c-TiO_2 when exposed to a short excitation wavelength (405 nm) from the substrate side (Figure S6c). This observation suggests that $Cs_2PbI_2Cl_2$ at the buried interface improved the extraction of electrons generated within the Cl-$CsPbI_3$ layer.

Device performance and stability

Figure 3A shows the PCE distribution for the PSCs fabricated using the $CsPbI_3$, Br-$CsPbI_3$, Cl-$CsPbI_3$, and Br/Cl-$CsPbI_3$ perovskite layers. The device structure consisted of FTO/c-TiO_2/perovskite/Spiro-OMeTAD/Au. The average PCE values of

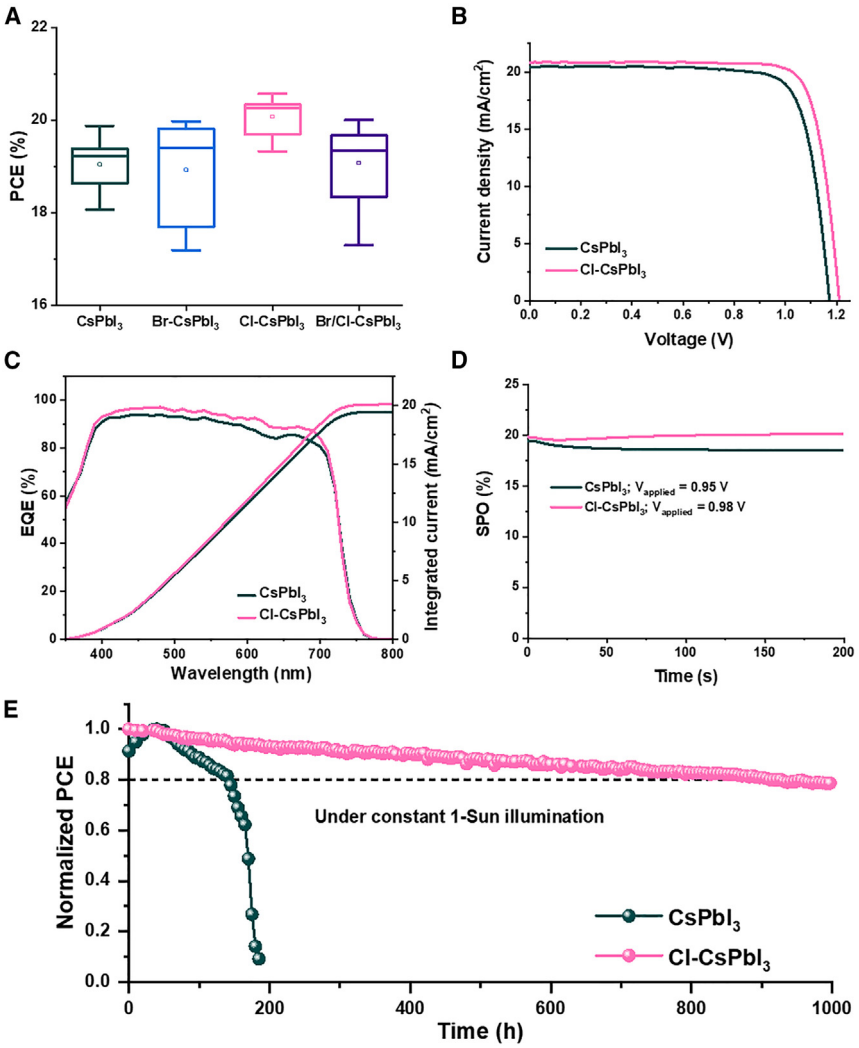

Figure 3. Solar cell performance and stability

(A) PCE distribution of 16 devices of $CsPbI_3$, Br-$CsPbI_3$, Cl-$CsPbI_3$, and Br/Cl-$CsPbI_3$ (center line, median; small square, mean; box, 25%–75% standard deviation; whiskers, outliers).

(B–E) *J-V* curves (B), EQE spectra and integrated J_{sc} (C), steady-state power output with applied voltage ($V_{applied}$) (D), and normalized PCE monitored as a function of exposure time (E) under 1-sun illumination of $CsPbI_3$ and Cl-$CsPbI_3$.

16 devices fabricated using the $CsPbI_3$, Br-$CsPbI_3$, Cl-$CsPbI_3$, and Br/Cl-$CsPbI_3$ perovskite layers were 18.9% ± 0.8%, 18.5% ± 2.1%, 20.1% ± 0.4%, and 18.6% ± 2.1%, respectively. The improvement in PCE from $CsPbI_3$ to Cl-$CsPbI_3$ can be attributed to the increase in the open-circuit voltage (V_{oc}) and fill factor (FF) (Figure S7), which results from the enhancements in charge extraction, crystallinity, and phase stability. Figure 3B shows the current density-voltage (*J-V*) characteristics of the best-performing devices of $CsPbI_3$ and Cl-$CsPbI_3$. The short-circuit current density (J_{sc}), V_{oc}, and FF values calculated from the *J-V* curve of the Cl-$CsPbI_3$-based device were 20.85 mA cm^{-2}, 1.21 V, and 82.0%, respectively, corresponding to a PCE of 20.6%, whereas the $CsPbI_3$-based device exhibited a PCE of 18.9% with J_{sc} = 20.46 mA cm^{-2}, V_{oc} = 1.17 V, and FF = 79.0%. The integrated J_{sc} calculated from the external quantum efficiency (EQE) of Cl-$CsPbI_3$ (20.10 mA cm^{-2}) was higher than that of $CsPbI_3$ (19.43 mA cm^{-2}), which is consistent

with the *J-V* characteristics (Figure 3C). We attributed the difference in the PCE performance to the interface modification because the surface morphology of the perovskite layers (Figure S8) and cross-sectional images of the devices prepared with $CsPbI_3$ and Cl-$CsPbI_3$ show no significant differences (Figure S9).

We also measured the stable power output (SPO) of one of the best-performing PSCs of $CsPbI_3$ and Cl-$CsPbI_3$ for 200 s at a fixed voltage near the maximum power point, which was obtained from the peaks of the *J-V* curves (Figure 3D). Under a constant applied voltage of 0.95 V, the PCE of the $CsPbI_3$-based device notably decreased from 19.2% to 17.9% after 200 s. In contrast, the PCE of the Cl-$CsPbI_3$-based device increased slightly from 19.8% to 20.1% at a constant applied voltage of 0.98 V for 200 s.

We conducted the light stability test on the unencapsulated devices under an ambient condition with an inert atmosphere (N_2), and constant 1-sun illumination (Figure 3E). The Cl-$CsPbI_3$-based device retained approximately 80% of its initial efficiency (the initial *J-V* curves and device parameters are presented in Figure S10) after continuous light exposure for 1,000 h, whereas the $CsPbI_3$-based device showed rapid degradation after 100 h.

EXPERIMENTAL PROCEDURES

Resource availability

Lead contact

Requests for further information and resources should be directed to and will be fulfilled by the lead contact, Prof. Hanul Min (hmin92@korea.ac.kr).

Materials availability

This study did not generate new unique reagents.

Data and code availability

All of the data associated with this study are included in the article and supplemental information. Additional information is available from the lead contact upon reasonable request.

Reagents and chemicals

All chemicals were of analytical grade and used as received without further purification.

Materials

The following materials were used: lead iodide (PbI_2; 99.99%, TCI), cesium iodide (CsI; 99.999%, Sigma-Aldrich), lead bromide ($PbBr_2$; Sigma-Aldrich), cesium chloride (CsCl; Sigma-Aldrich), DMAI (99%, Sigma-Aldrich), dimethyl formamide (DMF; 99.9%, Sigma-Aldrich), n-octylammonium iodide (OAI; Sigma-Aldrich), chlorobenzene (CB; 99.8%, Sigma-Aldrich), 2-propanol (IPA; 99.5%, Sigma-Aldrich), acetonitrile (ACN; 99%, Sigma-Aldrich), 4-tert-butylpyridine (t-BP; 98.0%, Sigma-Aldrich), lithium bis(trifluoromethanesulfonyl) imide (Li-TFSI; 99.0%, Sigma-Aldrich), Spiro-OMeTAD (Lumtech), and Co(III) bis(trifluoromethane) sulfonimide salt (FK209; Lumtech).

Preparation of the perovskite solutions

The perovskite precursor solution with a concentration of 0.8 M was obtained by dissolving stoichiometric amounts (1:1:1) of (PbI_2:CsI:DMAI) in DMF. For the Cl- and/or Br-containing $CsPbI_3$ precursor solution, 20 mol % of CsBr and/or 15 mol % of CsCl

replaced the same molar ratio of CsI. The solution was stirred at room temperature until it became transparent and then filtered with a 0.45-μm syringe filter.

Solar cell fabrication

Patterned FTO (12–15 Ω cm^{-2}, Asahi) glass substrates were sequentially washed with detergent, deionized (DI) water, acetone, and ethanol for 20 min each in an ultrasonic bath. The FTO glass substrates were then dried by blowing N_2 and then kept in the oven at 70°C for 1 h. For the c-TiO_2 layer, a 20 mM titanium diisopropoxide bis(acetylacetonate) (75 wt % in IPA) in ethanol (99.9%) was spray coated on the FTO at 450°C. After spray coating, the substrates with c-TiO_2 electron-transporting layer underwent plasma treatment and were preheated at 70°C prior to use for perovskite film coating. Perovskite films were fabricated by spin coating at 3,000 rpm for 30 s and then heated at 170°C for 20 m. All perovskite layers were surface passivated by OAI (3 mg/mL in IPA) and annealed at 100°C for 5 min. The Spiro-OMeTAD solution, which was prepared by mixing 94 mg mL^{-1} of Spiro-OMeTAD in CB with 38 μL of t-BP, 23 μL of Li-TFSI salt (520 mg mL^{-1} in ACN), and 9 μL of Co-TFSI salt (375 mg mL^{-1} in ACN), was spin coated at 3,500 rpm for 30 s. Finally, an 80 nm Au electrode was deposited on top of the Spiro-OMeTAD layer by a vacuum thermal evaporation system. For the measurement of high-efficiency devices, an antireflective film (Nanoeco-way) was applied to the glass surface. All experiments were performed in a dry room at an RH of 15%–35%.

Characterization

The optical properties of the perovskite films were measured using a Shimadzu UV-2600 single monochromatic UV-vis spectrophotometer with a wavelength range from 300 to 1,200 nm. The crystal structure of perovskite films was investigated using a SmartLab Rigaku XRD instrument. For XRD measurements, Cu radiation from an X-ray tube operated at a potential difference of 40 kV and 10 mA was used. Scanning electron microscopy images were obtained with a Hitachi Regulus 8220 ultra-high-resolution scanning electron microscope. The PL spectra were obtained from a Horiba Fluorolog-3 model FL3-22 spectrometer (Horiba Jobin Yvon) equipped with a 450-W xenon lamp and an R928P detector. The PL decay curves were recorded using the TCSPC technique on a Fluorolog-3 spectrometer (Horiba Jobin Yvon), and the excitation source was pulsed light. EQE curves were obtained using a McScience-K3100 solar cell quantum efficiency test system with a xenon lamp light source with a beam width of 1.2–10 mm. Preceding each measurement, a silicon diode with a known spectrum served as a reference standard. The *J–V* characteristics of the devices were measured under simulated 1.5-G irradiation (100 mV cm^{-2}) produced by a xenon lamp solar simulator (McScience class AAA) using a Keithley 2420 source meter. The scan speed, dwell time, mask area, and device contact area for the *J–V* characteristics were 20 mV/s, 0.01 s, 0.096 cm^2, and 0.203 cm^2, respectively. Air mass (AM) 1.5-G irradiation was calibrated with a standard Si cell (Newport, KG5 window). 3D distributions of ions in the devices were obtained by using a ToF-SIMS 5 (ION-TOF, Germany) equipped with a primary beam of 30 keV and 1 pA using a Bi^+ and Cs^+ sputter beam of 0.5 keV and 40 nA. The long-term light stability of unencapsulated devices was measured in the N_2 atmosphere with a 70-W metal halide lamp (Osram Powerball HCI-PAR30 70/942 NDL PB FL) by using a Keithley 2400 source meter unit. For the long-term light stability, the *J-V* measurement was conducted every 5 h.

SUPPLEMENTAL INFORMATION

Supplemental information can be found online at https://doi.org/10.1016/j.xcrp.2024.101935.

ACKNOWLEDGMENTS

This work was conducted under the framework of the Research and Development Program of the Korea Institute of Energy Research (KIER) (grants C3-2401 and C3-2402). H.M. acknowledges support from the National Research Foundation of Korea (RS-2023-00220077) and from the Korea Institute of Science and Technology (KIST) Institutional Program (2V09840). J.P. and S.I.S. acknowledge financial support from the Basic Science Research Program (NRF-2018R1A2A3074921).

AUTHOR CONTRIBUTIONS

H.M. designed and supervised the research. S.-F.-A.S. fabricated perovskite films and devices with supervision from J.H.P. and K.K. I.J., D.S., and I.H. characterized perovskite films. J.P. performed a preliminary experiment with supervision from S.I.S. H.M. wrote the draft of the manuscript, and all authors contributed feedback and comments for revising the manuscript.

DECLARATION OF INTERESTS

The authors declare no competing interests.

Received: December 12, 2023
Revised: March 11, 2024
Accepted: April 2, 2024
Published: April 25, 2024

REFERENCES

1. Wang, Y., Dar, M.I., Ono, L.K., Zhang, T., Kan, M., Li, Y., Zhang, L., Wang, X., Yang, Y., Gao, X., et al. (2019). Thermodynamically stabilized β-$CsPbI_3$–based perovskite solar cells with efficiencies >18%. Science *365*, 591–595. https://doi.org/10.1126/science.aav8680.

2. Li, Y., Li, R., and Lin, Q. (2022). Engineering the Non-Radiative Recombination of Mixed-Halide Perovskites with Optimal Bandgap for Indoor Photovoltaics. Small *18*, 2202028. https://doi.org/10.1002/smll.202202028.

3. Wang, K.-L., Lu, H., Li, M., Chen, C.-H., Bo Zhang, D.-., Chen, J., Wu, J.-J., Zhou, Y.-H., Wang, X.-Q., Su, Z.-H., et al. (2023). Ion–Dipole Interaction Enabling Highly Efficient CsPbI3 Perovskite Indoor Photovoltaics. Adv. Mater. *35*, 2210106. https://doi.org/10.1002/adma.202210106.

4. Yoon, S.M., Min, H., Kim, J.B., Kim, G., Lee, K.S., and Seok, S.I. (2021). Surface Engineering of Ambient-Air-Processed Cesium Lead Triiodide Layers for Efficient Solar Cells. Joule *5*, 183–196. https://doi.org/10.1016/j.joule.2020.11.020.

5. Gu, X., Xiang, W., Tian, Q., and Liu, S.F. (2021). Rational Surface-Defect Control via Designed Passivation for High-Efficiency Inorganic Perovskite Solar Cells. Angew. Chem. Int. Ed. Engl. *60*, 23164–23170. https://doi.org/10.1002/anie.202109724.

6. Mali, S.S., Patil, J.V., Shao, J.-Y., Zhong, Y.-W., Rondiya, S.R., Dzade, N.Y., and Hong, C.K. (2023). Phase-heterojunction all-inorganic perovskite solar cells surpassing 21.5% efficiency. Nat. Energy *8*, 989–1001. https://doi.org/10.1038/s41560-023-01310-y.

7. Cui, Y., Shi, J., Meng, F., Yu, B., Tan, S., He, S., Tan, C., Li, Y., Wu, H., Luo, Y., et al. (2022). A Versatile Molten-Salt Induction Strategy to Achieve Efficient CsPbI3 Perovskite Solar Cells with a High Open-Circuit Voltage >1.2 V. Adv. Mater. *34*, 2205028. https://doi.org/10.1002/adma.202205028.

8. Wang, J., Che, Y., Duan, Y., Liu, Z., Yang, S., Xu, D., Fang, Z., Lei, X., Li, Y., and Liu, S.F. (2023). 21.15%-Efficiency and Stable γ -CsPbI3 Perovskite Solar Cells Enabled by an Acyloin Ligand. Adv. Mater. *35*, 2210223. https://doi.org/10.1002/adma.202210223.

9. Duan, Y., Wang, J., Xu, D., Ji, P., Zhou, H., Li, Y., Yang, S., Xie, Z., Hai, X., Lei, X., et al. (2024). 21.41%-Efficiency CsPbI3 Perovskite Solar Cells Enabled by an Effective Redox Strategy with 4-Fluorobenzothiohydrazide in Precursor Solution. Adv. Funct. Mater. *34*, 2312638. https://doi.org/10.1002/adfm.202312638.

10. Xu, D., Wang, J., Duan, Y., Yang, S., Zou, H., Yang, L., Zhang, N., Zhou, H., Lei, X., Wu, M., et al. (2023). Highly-Stable CsPbI3 Perovskite Solar Cells with an Efficiency of 21.11% via Fluorinated 4-Amino-Benzoate Cesium Bifacial Passivation. Adv. Funct. Mater. *33*, 2304237. https://doi.org/10.1002/adfm.202304237.

11. Jeon, N.J., Noh, J.H., Yang, W.S., Kim, Y.C., Ryu, S., Seo, J., and Seok, S.I. (2015). Compositional engineering of perovskite materials for high-performance solar cells. Nature *517*, 476–480. https://doi.org/10.1038/nature14133.

12. Steele, J.A., Jin, H., Dovgaliuk, I., Berger, R.F., Braeckevelt, T., Yuan, H., Martin, C., Solano, E., Lejaeghere, K., Rogge, S.M.J., et al. (2019). Thermal unequilibrium of strained black $CsPbI_3$ thin films. Science *365*, 679–684. https://doi.org/10.1126/science.aax3878.

13. Lee, J.-W., Dai, Z., Han, T.-H., Choi, C., Chang, S.-Y., Lee, S.-J., De Marco, N., Zhao, H., Sun, P., Huang, Y., and Yang, Y. (2018). 2D perovskite stabilized phase-pure formamidinium perovskite solar cells. Nat. Commun. *9*, 3021. https://doi.org/10.1038/s41467-018-05454-4.

14. Kim, H., Lee, S.-U., Lee, D.Y., Paik, M.J., Na, H., Lee, J., and Seok, S.I. (2019). Optimal Interfacial Engineering with Different Length of Alkylammonium Halide for Efficient and Stable Perovskite Solar Cells. Adv. Energy Mater. *9*, 1902740. https://doi.org/10.1002/aenm.201902740.

15. Du, Y., Tian, Q., Wang, S., Yang, T., Yin, L., Zhang, H., Cai, W., Wu, Y., Huang, W., Zhang, L., et al. (2023). Manipulating the Formation of 2D/3D Heterostructure in Stable High-Performance Printable CsPbI3 Perovskite Solar Cells. Adv. Mater. *35*, 2206451. https://doi.org/10.1002/adma.202206451.

16. Zhao, X., Liu, T., Burlingame, Q.C., Liu, T., Holley, R., Cheng, G., Yao, N., Gao, F., and Loo, Y.-L. (2022). Accelerated aging of all-inorganic, interface-stabilized perovskite solar cells. Science *377*, 307–310. https://doi.org/10.1126/science.abn5679.

17. Liu, T., Zhao, X., Zhong, X., Burlingame, Q.C., Kahn, A., and Loo, Y.-L. (2022). Improved Absorber Phase Stability, Performance, and Lifetime in Inorganic Perovskite Solar Cells with Alkyltrimethoxysilane Strain-Release Layers at the Perovskite/TiO2 Interface. ACS Energy Lett. *7*, 3531–3538. https://doi.org/10.1021/acsenergylett.2c01610.

18. Min, H., Hu, J., Xu, Z., Liu, T., Khan, S.-U.-Z., Roh, K., Loo, Y.-L., and Rand, B.P. (2022). Hot-Casting-Assisted Liquid Additive Engineering for Efficient and Stable Perovskite Solar Cells. Adv. Mater. *34*, 2205309. https://doi.org/10.1002/adma.202205309.

19. Xu, D., Wang, J., Duan, Y., Yang, S., Zou, H., Yang, L., Zhang, N., Zhou, H., Lei, X., Wu, M., et al. (2023). Highly-Stable CsPbI3 Perovskite Solar Cells with an Efficiency of 21.11% via Fluorinated 4-Amino-Benzoate Cesium Bifacial Passivation. Adv Funct. Mater. *33*, 2304237. https://doi.org/10.1002/adfm.202304237.

20. Min, H., Lee, D.Y., Kim, J., Kim, G., Lee, K.S., Kim, J., Paik, M.J., Kim, Y.K., Kim, K.S., Kim, M.G., et al. (2021). Perovskite solar cells with atomically coherent interlayers on SnO2 electrodes. Nature *598*, 444–450. https://doi.org/10.1038/s41586-021-03964-8.

21. Li, J., Yu, Q., He, Y., Stoumpos, C.C., Niu, G., Trimarchi, G.G., Guo, H., Dong, G., Wang, D., Wang, L., and Kanatzidis, M.G. (2018). Cs2PbI2Cl2, All-Inorganic Two-Dimensional Ruddlesden–Popper Mixed Halide Perovskite with Optoelectronic Response. J. Am. Chem. Soc. *140*, 11085–11090. https://doi.org/10.1021/jacs.8b06046.

22. Xu, Z., Chen, M., and Liu, S.F. (2019). Layer-Dependent Ultrahigh-Mobility Transport Properties in All-Inorganic Two-Dimensional Cs2PbI2Cl2 and Cs2SnI2Cl2 Perovskites. J. Phys. Chem. C *123*, 27978–27985. https://doi.org/10.1021/acs.jpcc.9b09512.

23. Li, Z., Liu, X., Xu, J., Yang, S., Zhao, H., Huang, H., Liu, S.F., and Yao, J. (2020). 2D–3D Cs2PbI2Cl2–CsPbI2.5Br0.5 Mixed-Dimensional Films for All-Inorganic Perovskite Solar Cells with Enhanced Efficiency and Stability. J. Phys. Chem. Lett. *11*, 4138–4146. https://doi.org/10.1021/acs.jpclett.0c01134.

24. Yang, S., Liu, W., Han, Y., Liu, Z., Zhao, W., Duan, C., Che, Y., Gu, H., Li, Y., and Liu, S.F. (2020). 2D Cs2PbI2Cl2 Nanosheets for Holistic Passivation of Inorganic CsPbI2Br Perovskite Solar Cells for Improved Efficiency and Stability. Adv. Energy Mater. *10*, 2002882. https://doi.org/10.1002/aenm.202002882.

25. Min, H., Kim, M., Lee, S.-U., Kim, H., Kim, G., Choi, K., Lee, J.H., and Seok, S.I. (2019). Efficient, stable solar cells by using inherent bandgap of α-phase formamidinium lead iodide. Science *366*, 749–753. https://doi.org/10.1126/science.aay7044.

26. Akkerman, Q.A., Bladt, E., Petralanda, U., Dang, Z., Sartori, E., Baranov, D., Abdelhady, A.L., Infante, I., Bals, S., and Manna, L. (2019). Fully Inorganic Ruddlesden–Popper Double Cl–I and Triple Cl–Br–I Lead Halide Perovskite Nanocrystals. Chem. Mater. *31*, 2182–2190. https://doi.org/10.1021/acs.chemmater.9b00489.

27. Wang, Y., Liu, X., Zhang, T., Wang, X., Kan, M., Shi, J., and Zhao, Y. (2019). The Role of Dimethylammonium Iodide in CsPbI3 Perovskite Fabrication: Additive or Dopant? Angew. Chem. Int. Ed. Engl. *58*, 16691–16696. https://doi.org/10.1002/anie.201910800.

28. Noh, J.H., Im, S.H., Heo, J.H., Mandal, T.N., and Seok, S.I. (2013). Chemical Management for Colorful, Efficient, and Stable Inorganic–Organic Hybrid Nanostructured Solar Cells. Nano Lett. *13*, 1764–1769. https://doi.org/10.1021/nl400349b.

29. Ozturk, T., Akman, E., Shalan, A.E., and Akin, S. (2021). Composition engineering of operationally stable CsPbI2Br perovskite solar cells with a record efficiency over 17. Nano Energy *87*, 106157. https://doi.org/10.1016/j.nanoen.2021.106157.

30. Ye, F., Ma, J., Chen, C., Wang, H., Xu, Y., Zhang, S., Wang, T., Tao, C., and Fang, G. (2021). Roles of MACl in Sequentially Deposited Bromine-Free Perovskite Absorbers for Efficient Solar Cells. Adv. Mater. *33*, 2007126. https://doi.org/10.1002/adma.202007126.

31. Xu, J., Boyd, C.C., Yu, Z.J., Palmstrom, A.F., Witter, D.J., Larson, B.W., France, R.M., Werner, J., Harvey, S.P., Wolf, E.J., et al. (2020). Triple-halide wide–band gap perovskites with suppressed phase segregation for efficient tandems. Science *367*, 1097–1104. https://doi.org/10.1126/science.aaz5074.

32. Li, B., Yang, S., Han, H., Liu, H., Zhao, H., Li, Z., Xu, J., and Yao, J. (2023). Highly Efficient 2D/3D Mixed-Dimensional Cs2PbI2Cl2/CsPbI2.5Br0.5 Perovskite Solar Cells Prepared by Methanol/Isopropanol Treatment. Nanomaterials *13*, 1239.

33. Guo, S., Bu, K., Li, J., Hu, Q., Luo, H., He, Y., Wu, Y., Zhang, D., Zhao, Y., Yang, W., et al. (2021). Enhanced Photocurrent of All-Inorganic Two-Dimensional Perovskite Cs2PbI2Cl2 via Pressure-Regulated Excitonic Features. J. Am. Chem. Soc. *143*, 2545–2551. https://doi.org/10.1021/jacs.0c11730.

34. Saidaminov, M.I., Kim, J., Jain, A., Quintero-Bermudez, R., Tan, H., Long, G., Tan, F., Johnston, A., Zhao, Y., Voznyy, O., and Sargent, E.H. (2018). Suppression of atomic vacancies via incorporation of isovalent small ions to increase the stability of halide perovskite solar cells in ambient air. Nat. Energy *3*, 648–654. https://doi.org/10.1038/s41560-018-0192-2.

35. Kim, G., Min, H., Lee, K.S., Lee, D.Y., Yoon, S.M., and Seok, S.I. (2020). Impact of strain relaxation on performance of α-formamidinium lead iodide perovskite solar cells. Science *370*, 108–112. https://doi.org/10.1126/science.abc4417.